Environmental Science & Technology

Article

Cite This: Environ. Sci. Technol. 2018, 52, 12934−12942

pubs.acs.org/est

Intermediate Volatility Organic Compound Emissions from a Large Cargo Vessel Operated under Real-World Conditions

Cheng Huang,*[,†] Qingyao Hu,[†] Yingjie Li,[†] Junjie Tian,[‡] Yingge Ma,[†] Yunliang Zhao,[§,∥,#] Jialiang Feng,[⊥] Jingyu An,[†] Liping Qiao,[†] Hongli Wang,[†] Sheng'ao Jing,[†] Dandan Huang,[†] Shengrong Lou,[†] Min Zhou,[†] Shuhui Zhu,[†] Shikang Tao,[†] and Li Li*[,†,⊥]

[†]State Environmental Protection Key Laboratory of Cause and Prevention of Urban Air Pollution Complex, Shanghai Academy of Environmental Sciences, Shanghai, 200233, China

[‡]School of Resources and Environment Engineering, East China University of Science and Technology, Shanghai, 200237, China

[§]Center for Atmospheric Particle Studies, Carnegie Mellon University, 5000 Forbes Avenue, Pittsburgh, Pennsylvania 15213, United States

[∥]Department of Mechanical Engineering, Carnegie Mellon University, 5000 Forbes Avenue, Pittsburgh, Pennsylvania 15213, United States

[⊥]Institute of Environmental Pollution and Health, Shanghai University, Shanghai, 200244, China

Supporting Information

ABSTRACT: Intermediate volatility organic compound (IVOC) emissions from a large cargo vessel were characterized under real-world operating conditions using an on-board measurement system. Test ship fuel-based emission factors (EFs) of total IVOCs were determined for two fuel types and seven operating conditions. The average total IVOC EF was 1003 ± 581 mg·kg-fuel^{-1}, approximately 0.76 and 0.29 times the EFs of primary organic aerosol (POA) emissions from low-sulfur fuel (LSF, 0.38 wt % S) and high-sulfur fuel (HSF, 1.12 wt % S), respectively. The average total IVOC EF from LSF was 2.4 times that from HSF. The average IVOC EF under low engine load (15%) was 0.5−1.6 times higher than those under 36%−74% loads. An unresolved complex mixture (UCM) contributed 86.1 ± 1.9% of the total IVOC emissions. Ship secondary organic aerosol (SOA) production was estimated to be 546.5 ± 284.1 mg·kg-fuel^{-1}; IVOCs contributed 98.9 ± 0.9% of the produced SOA on average. Fuel type was the dominant determinant of ship IVOC emissions, IVOC volatility distributions, and SOA production. The ship emitted more IVOC mass, produced higher proportions of volatile organic components, and produced more SOA mass when fueled with LSF than when fueled with HSF. When reducing ship POA emissions, more attention should be paid to commensurate control of ship SOA formation potential.

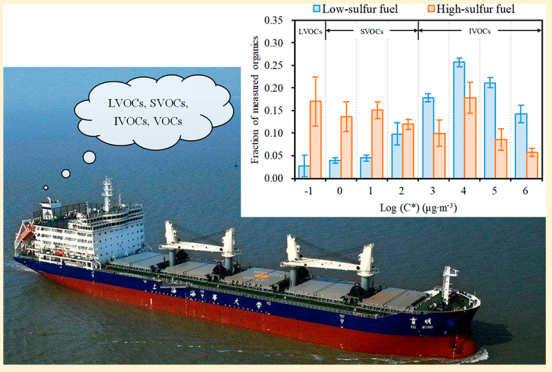

INTRODUCTION

Ship emissions have attracted increasing attention due to their potential impacts on the atmospheric environment and public health.[1−6] Field measurements indicate that ship emissions contribute substantially to ambient particulate matter in coastal areas.[7−10] Marine vessels are primarily fueled with heavy fuel oil (HFO), which emits numerous gaseous and particulate species, including organic matter (OM), black carbon (BC), sulfate, and criteria pollutants such as SO_2, NO_x and PM.[11−15] OM is one of the most abundant components in ship emissions, particularly in the exhaust of ships burning low sulfur fuel (LSF), in which OM exceeds sulfate and is the primary pollutant.[15−17]

Whereas particulate organic matter (POM) emissions are significant, considerable amounts of intermediate volatile organic compounds (IVOCs) have also been detected in ship exhaust in previous studies.[18,19] IVOCs include species with effective saturation concentrations between 10^3 and 10^6 $\mu g \cdot m^{-3}$, which roughly corresponds to the volatility range of C12−C22 *n*-alkanes.[20,21] Laboratory experiments indicate that individual IVOCs (e.g., polycyclic aromatic hydrocarbons and linear, branched, and cyclic alkanes) can form secondary organic aerosol (SOA) with high yields.[22−26] IVOCs released from gasoline and diesel vehicles have been found to be important SOA precursors in urban atmospheres.[27−30] Zhao et al.[31,32] reported total amounts and chemical compositions of IVOC emitted from gasoline and diesel vehicles, which can be used to quantify SOA production from on-road vehicle IVOCs.

Received: August 8, 2018
Revised: October 5, 2018
Accepted: October 16, 2018
Published: October 16, 2018

DOI: 10.1021/acs.est.8b04418
Environ. Sci. Technol. 2018, 52, 12934−12942

The techniques commonly used to measure volatile organic compounds (VOCs) and organic aerosol (OA) cannot be used to quantify IVOCs,[33] and the majority of IVOC emissions cannot be speciated using traditional chromatography-based techniques.[34] Previous studies have estimated total IVOC emissions by scaling measured hydrocarbon or primary organic aerosol (POA) emissions.[27,35−38] However, these estimates compare poorly with measured data.[31,32] Recently, Zhao et al.[34] developed an IVOCs quantification method involving gas chromatography/mass spectrometry (GC/MS) analysis of adsorbed IVOC samples; this method was used to quantify unspeciated IVOCs, which were used in turn to determine the emission factors (EFs) and chemical compositions of IVOCs emitted from gasoline- and diesel-fueled on-road vehicles and gasoline-fueled off-road engines.[31,32]

International shipping is a globally important source of air pollutant emissions,[39] and shipping emissions have increased with recent growth in global maritime trade.[40,41] To address ship emissions, the International Maritime Organization (IMO) has gradually tightened the fuel sulfur content (FSC) limits for ships. The FSC has been restricted to 0.1% in sulfur emission control areas (SECAs) in European and North American coastal waters since 2015, and will be more widely restricted to 0.5% in international waters beginning in 2020.[42] Emissions of most pollutants produced by ships have decreased due to the transition from HFO to distillate fuel (DF).[17,43−45] However, emissions of gaseous organic compounds have not decreased significantly; in fact, some aromatic species, such as toluene, phenanthrene, and naphthalene, have increased.[18,19] One field measurement campaign in a coastal city indicated that SOA load can increase substantially under the influence of local ship emissions.[46] Quantifying IVOC emissions from ships is therefore of great importance in accurately assessing the impact of anthropogenic sources on SOA. However, due to the lack of measurement, quantitative information on IVOC emissions from ships, especially under real-world operating conditions are largely unknown at present.

In this study, total (speciated and unspeciated) IVOC emissions from a large bulk carrier were measured under real-world operating conditions via on-board measurements. The mass, volatility, and chemical composition of IVOCs from the ship were determined under various operating modes, including at-berth, maneuvering, and cruising. The relationships between total IVOC emissions and emissions of hydrocarbons and POA were investigated. SOA production from the measured IVOCs was predicted and compared with estimates of gasoline and diesel exhaust SOA formation from previous studies.

EXPERIMENTAL PROCEDURES

Test Ship and Fuels. In this study, measurements were performed on a Handysize class bulk carrier built in 2012 with a dead weight of 45 308 t and gross tonnage of 31 113 t. Bulk carrier is the main type of ocean-going and coastal ships in East Asia, accounting for 21% of the register number of ships.[3] The ship has one main engine, four auxiliary engines, and an auxiliary boiler. The main engine is a MAN B&W 6S50ME-C8 two-stroke low-speed diesel engine with a maximum power of 7948 kW and rated speed of 127 rpm. The auxiliary engine is a MAN B&W 6L16/24, a four-stroke medium-speed diesel engine with a maximum power of 660 kW, and rated speed of 1200 rpm. China has executed legislation that requires ships to use low-sulfur fuel (LSF, < 0.5 wt %S) when at-berth since January 1, 2017. Apart from that, high-sulfur fuel (HSF) is commonly used for ocean-going and coastal ships in China. In this study, both the main and auxiliary engines were fueled with RMG 180-grade HFO during the test. When at-berth, the main and auxiliary engines burned LSF with 0.38 wt % S, then switched to HSF with 1.12 wt % S during the subsequent voyage. It should be mentioned that LSF was also used by the main engine during departure from the port although HSF was allowed by the current policy in Chinese SECAs. Fuel details are presented in Supporting Information Table S1.

Test Procedures. Measurements were conducted throughout a July 2017 voyage across a number of Chinese seas. The ship traveled sequentially through Bohai Bay, the Yellow Sea, the East China Sea, and eventually into the Yangtze River. In total, eleven exhaust samples were collected from the test ship under typical operating conditions, including at-berth, maneuvering, and cruising at sea. Specifically, one sample was collected from an auxiliary engine when at-berth, while the other ten samples were collected from the main engine when the ship was maneuvering or cruising at sea. Two samples were collected during departure (once from port and once from anchor), one sample was collected during arrival, and the other seven samples were collected during cruising. During cruising sampling, the ship was manually operated at four different speeds corresponding to four engine loads (74%, 51%, 36%, and 15%) to investigate the impact of engine load on emissions. A detailed description of the test procedures is provided in SI Section S1. The measurement campaign voyage and ship operating conditions during each sampling period are presented in Figure S1 and Table S2, respectively.

Sampling and Analysis. The ship has six separated chimneys at about 10 m above the deck. One for the main engine, four for the auxiliary engines, and the other one for the auxiliary boiler. During sampling, we installed the sampling instruments separately on the chimney of the main engine and auxiliary machine in turn. The exhaust was partially diverted to the deck level through a stainless-steel duct with an internal diameter of 108 mm. The sampling ports were located approximately 15 m downstream from the chimney. To avoid IVOC condensation and particle precipitation, a thermal insulating sleeve was wrapped around the outside of the duct to maintain an exhaust temperature of ∼150 °C. A schematic diagram of the sampling setup is shown in Figure S2. The sampling port featured two channels: one leading to a dilution system and the other leading to a raw gaseous-species analyzer. Both sample types were collected through straight multiholed probes constructed from stainless steel and extending across the exhaust duct. In one channel, the exhaust was diluted by a Dekati FPS 4000 dilution system with HEPA-filtered and carbon-adsorbed compressed air before sampling. Both the exhaust sample and dilution air were heated to 180−200 °C to maintain the temperature of the exhaust to avoid condensation due to rapid decrease of exhaust temperature. The test-average dilution ratios were ∼64:1 during the first two sampling; the other samples featured ratios of ∼8:1 (Table S2). The diluted exhaust stream was collected on filters, in stainless-steel canisters, and in thermal desorption (TD) tubes for various analyses. The canisters and TD tubes sampled the diluted exhaust via Teflon tubes. After dilution, the exhaust temperature was about 40−50 °C, and the filters and TD tube sampling train were maintained at the same temperature during sampling.

DOI: 10.1021/acs.est.8b04418
Environ. Sci. Technol. 2018, 52, 12934−12942

IVOCs were sampled by drawing dilute exhaust through a quartz filter immediately followed by a TD tube (6 mm internal diameter (i.d.) × 100 mm length) that contained absorbents consisting of (from weak to strong) 10 mm of quartz wool, 10 mm of Tenax TA (35/60 mesh), and 10 mm of Carbograph 5TD (40/60 mesh) from Markes International Ltd. (Liantrisant, UK). Prior to initial use, the TD tubes were subjected to a cleanup at 320 °C for 1 h at a flow rate of 100 mL/min, then sealed with long-term storage caps, wrapped in aluminum foil, and stored in a refrigerator at 4 °C. Pocket air sampling pumps (210−1000 MH, SKC, Houston, TX, USA) were used for sample collection at a nominal flow rate of 100 mL·min^{-1}. The actual flow rate of the pump was calibrated using a digital flow meter (Sensidyne Gilian Gilibrator, St. Petersburg, FL, USA) before and after sampling. All samples were placed in a cooling box, transported to the laboratory, stored in a freezer at −18 °C, and analyzed within a month.

TD tubes were analyzed using a TD-GC/MS system.[47] Prior to analysis, a known amount of deuterated standards (d_8-naphthalene, d_{10}-acenaphthene, d_{10}-phenanthrene, d_{18}-octane, d_{26}-dodecane, and d_{40}-nonadecane) were injected into each adsorbent tube to determine the recoveries of the various IVOCs during analysis. Nineteen individual IVOC compounds were quantified using authentic standards. The analytical methods are detailed in SI Section S2. Detection of a peak in the samples was based on a signal-to-noise ratio of 3 or greater. Internal standard quantification method was used to determine the amounts of targets in the samples; detailed calculation is also provided in SI Section S2. Repeatability was evaluated by assessing the relative standard deviation (RSD) of replicate tubes (n = 5) with the value below 20%. Desorption recovery (DR) (97−100%) was defined as the percentage of amount detected from the first sample run divided by the sum of amount from the first and second sample runs. To evaluate the breakthrough of TD tubes during sampling, a pre-experiment was conducted on the test ship by using two TD tubes connected in series before the formal test. The first tube was spiked with five internal standards used in the study at 1 ng/tube d_8-naphthalene, d_{10}-acenaphthene, and d_{10}-phenanthrene, and at 3 ng/tube d_{26}-dodecane and d_{40}-nonadecane. The second tube was blank. The sample was collected from an auxiliary engine of the test ship when it was docked in the port. The test sequences followed the same procedure as with the formal test described above. The sampling time was 45 min. After sampling, the second tube was analyzed; d_{26}-dodecane, d_8-naphthalene, and other internal standard compound were not detected in the back up tubes, which indicated no breakthrough during this collection.

For each test, PM samples were collected on two Teflon filters (47-mm, TE38, Whatman, UK) and two quartz filters (47-mm, QM-A, Whatman, UK) (Figure S2). The Teflon filter samples were subsequently analyzed gravimetrically in the laboratory for particulate mass. One quartz filter sample was analyzed for organic carbon (OC) and elemental carbon (EC) content using a Desert Research Institute (DRI) thermal/optical carbon analyzer model 2001 following the IMPROVE-A protocol.[48] POA was estimated by multiplying the measured OC by 1.2.[49] VOC species emissions were sampled in SUMMA canisters and analyzed offline for individual C2 to C11 hydrocarbons using a gas chromatograph with a mass spectrometer and a flame ionization detector (GC-MS/FID). The PM and VOC analysis techniques are detailed in our previous study.[15] A Horiba OBS 2200 portable emission measurement system (PEMS) was used to analyze the raw exhaust gas for total hydrocarbon (THC), nitrogen oxide (NO_x, which includes NO and NO_2), CO, and CO_2. THC was evaluated using flame ionization detection (FID), NO and NO_2 were measured via chemiluminescent detection (CLD), and CO and CO_2 were measured using nondispersive infrared detection (NDIR).

Quantification of IVOCs. The total IVOC mass (speciated + unresolved complex mixture, or UCM) was determined using the approach outlined in Zhao et al.,[34] and the detailed calculation method is provided in SI Section S3. Briefly, the total ion signal from each adsorbent sample was separated into 11 bins based on retention time during the GC analysis. The retention time associated with each bin number is shown in Table S4. Bins corresponding to given C_n n-alkanes were designated B_n, where "n" denotes the n-alkane carbon number. The resolved compounds included straight-chain alkanes (n-alkanes), branched alkanes (b-alkanes), and polycyclic aromatic hydrocarbons (PAHs). The UCM IVOCs in each retention-time-based IVOC bin were further classified into unspeciated b-alkanes and unspeciated cyclic compounds with reference to Zhao et al.[31,32] Quartz filter samples were also analyzed via an Agilent GC/MS system under the same method used for the IVOCs. Detailed methods are provided in SI Section S4. As shown in Figure S4, the POA emissions measured by the GC/MS analysis are clearly related to those measured by the OC/EC analyzer.

Emission Factor Calculations. IVOC emissions are reported as fuel-based EFs (mg·kg-fuel^{-1}), which were calculated using the carbon-mass-balance approach as shown in eq 1.

$$\mathrm{EF_{IVOCs}} = \frac{[\mathrm{IVOCs}] \times f_c}{\Delta \mathrm{CO_2} + \Delta \mathrm{CO} + \Delta \mathrm{PM_C} + \Delta \mathrm{THC}} \quad (1)$$

where [IVOCs] is the measured mass concentration of the IVOC species (μg·m^{-3}), and f_c is the mass fraction of carbon (%) in the fuel as determined by the fuel analysis (see Table S1). ΔCO_2, ΔCO, ΔPM_C, and ΔTHC are the background-corrected carbon concentrations in CO_2, CO, carbonaceous PM, and THC. Figure 1 shows the total IVOC EFs in each retention-time bin for samples no. 2 (a) and no. 4 (b) from the main engine fueled by LSF and HSF. The total IVOC signal appears to consist predominantly of an UCM. Unlike IVOC emission distributions from gasoline or diesel vehicles,[31,32] the test ship IVOC emissions feature two peaks, which are located at retention times of 18−19 min and 21−22 min, corresponding to the B_{14} and B_{18}−B_{19} IVOC bins, respectively. High-carbon-number IVOC emissions are higher when using HSF than when using LSF.

RESULTS AND DISCUSSION

IVOC Emission Factors. Figure 2a shows the total IVOC EFs for the test ship under different operating conditions. Ship IVOC emissions are primarily controlled by the fuel type. The average IVOC EF when the ship is fueled by LSF is 2052 ± 282 mg·kg-fuel^{-1}, which is roughly 2.4 times the HSF-fueled IVOC EF. The operating conditions also influence ship IVOC emissions. When the ship was cruising at sea, the IVOC EF at low load (15%) was relatively higher, about 0.5−1.6 times higher than those produced at loads of 36%−74% (data shown in Table S6). This trend is consistent with the changes in THC and POA emissions from the test ship (as revealed by OC/EC

DOI: 10.1021/acs.est.8b04418
Environ. Sci. Technol. 2018, 52, 12934−12942

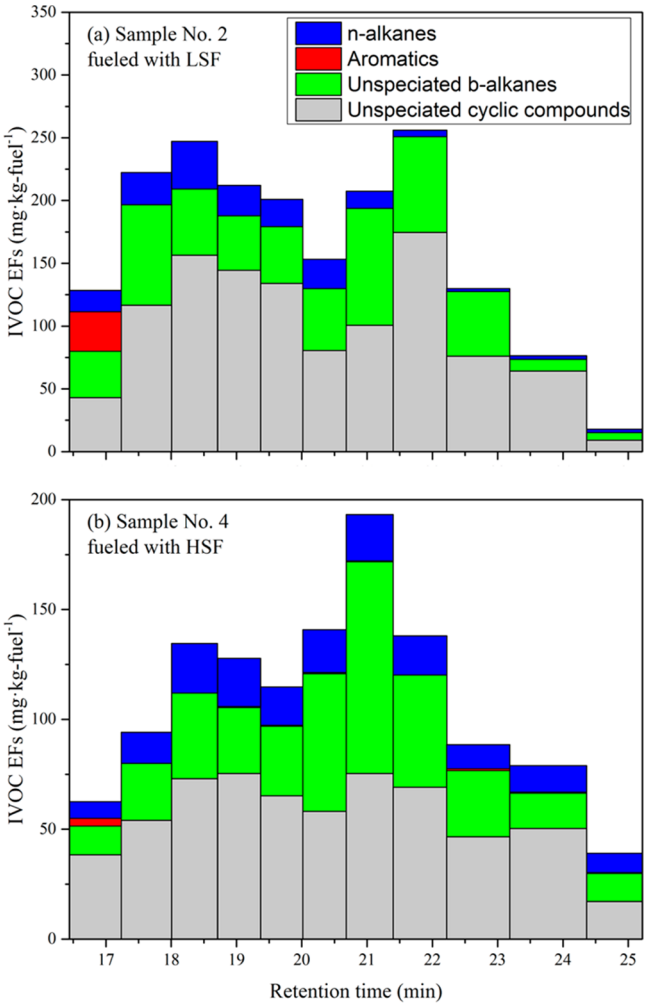

Figure 1. EFs of quantified IVOC components in each retention-time bin for samples no. 2 and no. 4 from the test ship main engine fueled with (a) LSF and (b) HSF.

analysis; Table S5) and also agree with published THC and OC emissions data for ocean-going ships.[11,15]

Figure 2b compares the total IVOC EFs from the test ship in this study with those measured in previous studies for diesel and gasoline vehicles.[31,32] The average test ship IVOC EF is 1003 ± 581 mg·kg-fuel^{-1}, which is similar to the average IVOC EF for diesel vehicles, but much higher than that for gasoline vehicles. It should be noted that the test sample size in this study is limited compared with those in previous diesel and gasoline vehicle studies. Additional measurements would be helpful for exploring variability in IVOC emissions from ocean-going ships.

IVOC Chemical Compositions. Figure 3a compares the chemical compositions of IVOC emitted by the test ship under different operating conditions (data shown in Table S6). *n*-Alkane and aromatic speciated IVOCs contribute 12.8 ± 1.9% and 1.1 ± 0.6% of the total IVOC emissions, respectively. Naphthalene dominates the speciated aromatic IVOC emissions, accounting for 56.0 ± 19.4% of the total aromatics. Unspeciated IVOCs account for 86.1 ± 1.9% of the total IVOC emissions, and unspeciated cyclic compounds are the dominant class of IVOCs, contributing 55.3 ± 3.5% of the total IVOC emissions. Fuel type has little influence on the emitted IVOC chemical composition, with the exception of aromatics, which feature higher mass fractions under LSF fueling (2.4 ± 0.4%) than under HSF fueling (0.8 ± 0.3%). The mass fraction contribution of naphthalene to total aromatics is also much higher from LSF (82.2 ± 1.2%) than from HSF (50.2 ± 16.1%), which is consistent with results from previous studies.[18,19]

Figure 3b compares the chemical compositions of IVOC emissions from the test ship with those from diesel and gasoline vehicles in previous studies.[31,32] The test ship *n*-alkane mass fraction (of total IVOC emissions) is much higher than those for diesel and gasoline vehicles. The test ship aromatic mass fraction (of total IVOC emissions) is similar to that for diesel vehicles, but much lower than that for gasoline vehicles. In addition, the test ship features a higher fraction of unspeciated *b*-alkanes and lower fraction of unspeciated cyclic compounds than the diesel and gasoline vehicles. These results indicate that the chemical composition of IVOC emissions from ocean-going ships is quite different from those of diesel and gasoline vehicle emissions. The IVOC composition is partially affected by fuel composition. HFO usually has much higher carbon numbers and lower combustion efficiency than diesel and gasoline, resulting in higher mass fractions of unburned *n*-alkanes in ship exhaust. However, we did not analyze the organic composition of fuel used in this study. Further fuel analysis may elucidate the formation mechanisms behind ship IVOC emissions.

Total Organics and Volatility Distributions. By combining the GC/MS data from the quartz filters and TD tubes, one can construct volatility distributions for IVOCs (C* = 300 to 3 × 10^6 μg·m^{-3}), semivolatile organic compounds (SVOCs, C* = 0.3−300 μg·m^{-3}), and low-volatility organic compounds (LVOCs, C* < 0.3 μg·m^{-3}) using the effective saturation concentration (C*) of the *n*-alkane in each bin. Figure 4 presents the volatility distributions of organics desorbed from quartz filters and TD tubes sampled from the test ship when fueled with LSF and HSF. The organics collected by the quartz filters (including IVOCs, SVOCs, and LVOCs) dominate the test ship total organics. Fuel type largely determines the organic volatility distribution. When fueled with LSF, IVOCs account for the majority (78.9 ± 1.1%) of the total organic emissions with C* values of less than 3 × 10^6 μg·m^{-3} (IVOCs + SVOCs + LVOCs), followed by SVOCs (18.3 ± 1.2%) and LVOCs (2.8 ± 2.4%). When fueled with HSF, the IVOC fraction decreases to 42.2 ± 7.5%, while the SVOC and LVOC fractions increase to 40.8 ± 2.3% and 17.0 ± 5.4%, respectively. The IVOC fraction from the HFO-fueled ship is less than that found for diesel vehicles,[31] while the SVOC and LVOC fractions are much higher. The volatility of the fuel itself may largely explain this difference. HFO usually contains a considerable amount of high-boiling-point impurities and asphaltites, including heterocyclic compounds, which result in large amounts of low-volatility and nonvolatile organic emissions from ships. This result also implies that although the use of LSF can reduce POA emissions, it may lead to an increase in IVOC emissions, which may contribute to greater eventual SOA production.

Quartz filter GC/MS measurements can only recover organic components in volatility bins with Log (C*) values greater than −1. For the same samples, the GC/MS analysis recovered an average of 51.8 ± 8.4% of the organics measured by the OC/EC analyzer; these recoveries are similar to those of filter samples collected from diesel exhaust.[31] During LSF- and HSF-fueled periods, 36.2 ± 1.9% and 42.5 ± 8.5%,

DOI: 10.1021/acs.est.8b04418
Environ. Sci. Technol. 2018, 52, 12934−12942

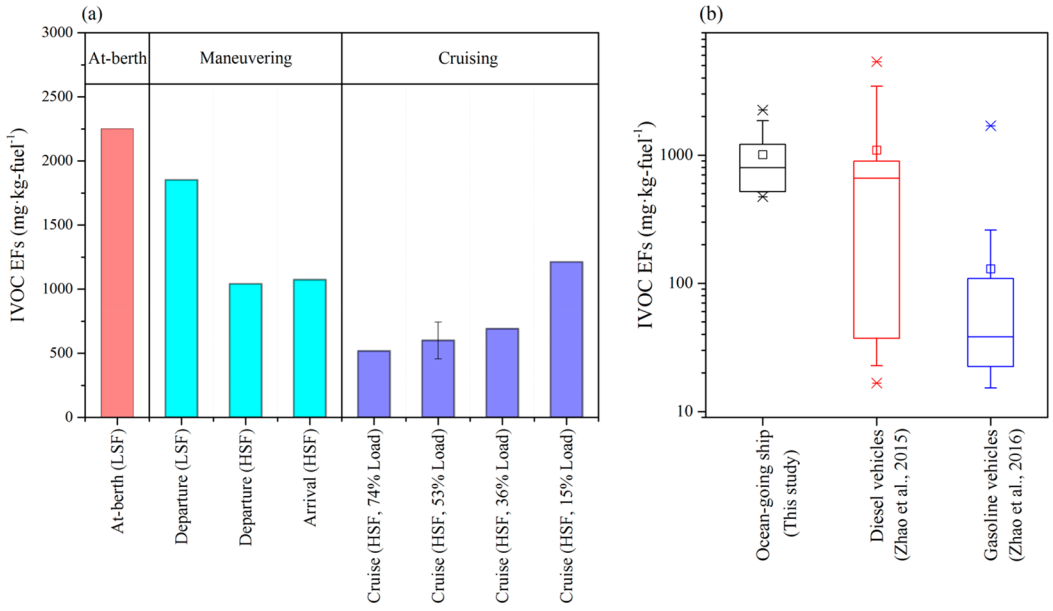

Figure 2. (a) Total test ship IVOC EFs under various operating conditions, including at-berth (red bar), maneuvering (blue bars), and cruising (purple bars); (b) box-whisker plots of total IVOC EFs for the ocean-going ship herein (black), diesel vehicles (red), and gasoline vehicles (blue). The boxes represent the 75th and 25th percentiles, the centerline is the median, and the whiskers are the 90th and 10th percentiles. The asterisks indicate the minimum and maximum IVOC EFs.

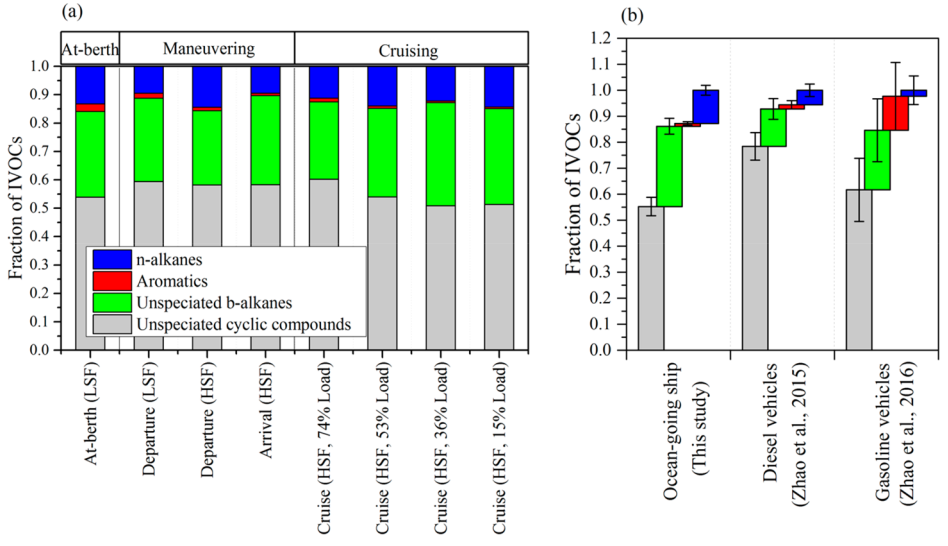

Figure 3. (a) Chemical composition of IVOCs, including *n*-alkanes (blue), aromatics (red), unspeciated *b*-alkanes (green), and unspeciated cyclic compounds (gray) for the test ship under different operating conditions; (b) comparison of IVOC chemical compositions for the ocean-going test ship herein and diesel and gasoline vehicles in previous studies. The error bars in (b) represent the standard deviation from the mean for the given chemical component.

respectively, of organics (including the organics measured on the quartz filters and TD tubes by GC/MS analysis) remain unrecovered. Table 1 shows the fractions of total organics in each volatility basis set (VBS) bin when the ship was fueled with LSF and HSF.

Relationships among Total IVOCs, POA, and THC. The IVOC and POA (from OC/EC analysis) EFs are correlated under various operating conditions. For HSF, the linear regression yields a slope (average IVOC-to-POA ratio) of 0.29 ± 0.06 and an R^2 of 0.64 (Figure S5). The IVOC and THC EFs have a weaker relationship, with an average IVOC-to-THC ratio of 0.67 ± 0.20 and R^2 of 0.23. During LSF-fueled periods, the average IVOC-to-POA and IVOC-to-THC ratios are 0.76 ± 0.00 and 1.54 ± 0.94, respectively, much higher than the slopes found for HSF. Unlike in gasoline or diesel exhaust,[31,32] IVOCs are better correlated with POA than with THC. This is mainly because a large fraction of IVOCs is adsorbed on quartz filters due to high organic aerosol loadings in ship's exhaust. Especially for HSF, the IVOCs measured on quartz filters accounted for ~60% of the total, as shown in Figure 4. The use of stainless-steel duct may also induce some IVOC losses owing to adsorption.

Figure S6 shows the THC mass closure under different fuel type and operating conditions. Speciated VOCs constitute 24.5%−34.3% and 2.1%−11.4% of the THC mass when the ship is fueled with LSF and HSF, respectively. The results from

DOI: 10.1021/acs.est.8b04418
Environ. Sci. Technol. 2018, 52, 12934−12942

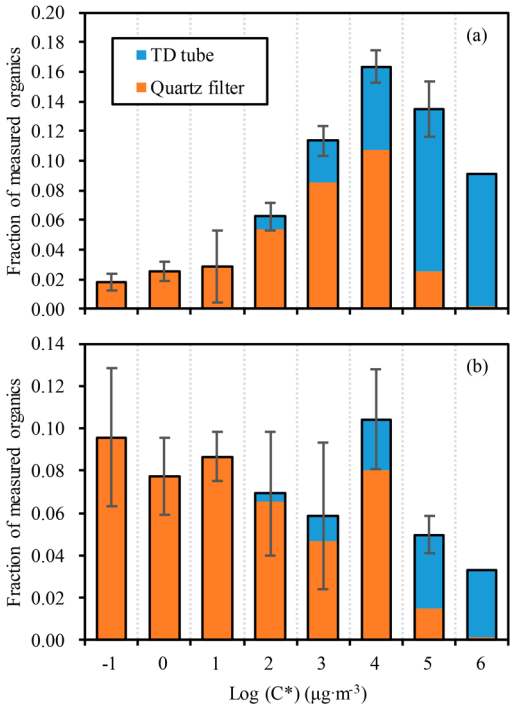

Figure 4. Volatility distribution of organics desorbed during GC/MS analysis of quartz filters and adsorbent tubes collected from the test ship when fueled with (a) LSF and (b) HSF. The distribution is expressed as the mass fraction of total organics in the 10^{-1} to 10^{6} $\mu g \cdot m^{-3}$ bins. The error bars represent the standard deviations of total organics. The orange bars are the average mass fractions of organics collected by the quartz filters; the blue bars show the average mass fractions of organics collected by the TD tubes.

Table 1. Mass Fractions of Total Organics Measured by GC/MS Analysis (Including Quartz Filter and TD Tube Samples) in Each VBS Bin, along with the Unrecovered OA (Log (C*) < −1) Mass Fraction

Log (C*)	LSF	HSF
<−1	36.2 ± 1.9%	42.5 ± 8.6%
−1	1.8 ± 1.6%	9.6 ± 3.0%
0	2.6 ± 0.4%	7.8 ± 1.8%
1	2.9 ± 0.5%	8.7 ± 1.7%
2	6.2 ± 1.4%	6.9 ± 1.6%
3	11.4 ± 0.3%	5.8 ± 2.6%
4	16.4 ± 0.1%	10.4 ± 3.2%
5	13.5 ± 0.3%	5.0 ± 1.6%
6	9.1 ± 1.5%	3.3 ± 0.7%

LSF are similar to those from diesel fuel, more than 70% of THC mass is unidentifiable by the VOC speciation analysis.[50] HSF usually contains more high carbon components which cannot be identified by traditional chromatography-based techniques, resulting in more than 90% in THC mass cannot be identified as individual VOCs in HSF's exhaust. Even when gas-phase IVOCs are taken into account, only 20.4%−51.7% of the THC mass can be explained, much lower than the speciated fraction by VOCs and IVOCs (~70%) in gasoline exhaust reported by Zhao et al.[51] The main reason is ~60% of the IVOCs is adsorbed on quartz filters as particulate-phase. If IVOCs on quartz filters were considered, the fraction of VOCs and IVOCs in THC mass could reach 48.9%−108.6%. Therefore, IVOC emissions from ships fueled with HFO are mainly determined by POA emissions. Thus, the use of POA to estimate total IVOC emissions from ships is recommended.

Estimation of SOA Production. On the basis of the measured test ship IVOC and VOC emissions, the SOA production from the total IVOCs and single-ring aromatics can be estimated using the following equation.[32]

$$\mathrm{SOA} = \sum ([\mathrm{HC}]_i \times (1 - e^{-k_{\mathrm{OH},i} \times [\mathrm{OH}] \times \Delta t}) \times Y_i) \quad (2)$$

where $[\mathrm{HC}]_i$ is the emission factor of SOA precursor i ($\mathrm{mg \cdot kg\text{-}fuel^{-1}}$); $k_{\mathrm{OH},i}$ is the OH reaction rate constant of precursor i at 25 °C ($\mathrm{cm^3 \cdot molecules^{-1} \cdot s^{-1}}$); [OH] is the OH concentration ($\mathrm{molecules \cdot cm^{-3}}$), which is assumed in this study to be 1.5×10^6 $\mathrm{molecules \cdot cm^{-3}}$; Δt is the photochemical age (h); and Y_i is the SOA mass yield of precursor i under high-NO_x conditions at an OA concentration of 20 $\mu g \cdot m^{-3}$. The SOA yields of the precursors were derived from Zhao et al.[31,32] The POA and IVOC emissions were corrected based on OA gas−particle partitioning behavior before estimating the SOA production. The POA EF ($\mathrm{EF_{POA}}$) can be predicted using absorptive partitioning theory,[20] as shown in eq 3.

$$\mathrm{EF_{POA}} = \mathrm{EF_{total}} \sum_i f_i \left(1 + \frac{C_i^*}{C_{\mathrm{OA}}}\right)^{-1} \quad (3)$$

where $\mathrm{EF_{total}}$ is the total organic aerosol EF in both the gas- and particle-phases ($\mathrm{mg \cdot kg\text{-}fuel^{-1}}$), f_i is the mass fraction of species i, C_{OA} is the organic aerosol mass concentration (20 $\mu g \cdot m^{-3}$), and C_i^* is the effective saturation concentration of species i ($\mu g \cdot m^{-3}$).

Figure 5a shows the POA emissions and predicted SOA production for the test ship under various operating conditions after 48 h of photo-oxidation. POA emissions are higher than the SOA production under all operating conditions. Nevertheless, the SOA formation potential of the ship emissions cannot be ignored. The test ship average SOA production is 546.5 ± 284.1 $\mathrm{mg \cdot kg\text{-}fuel^{-1}}$, which is higher than the average SOA production estimated by Zhao et al.[31] for diesel vehicles without exhaust after-treatments. Fuel type influences SOA production considerably. The average SOA production reaches 958.0 ± 132.0 $\mathrm{mg \cdot kg\text{-}fuel^{-1}}$ when the test ship is fueled with LSF, which is ~1.6 times higher than the SOA production during HSF use. Previous studies have indicated that organic emissions from ships can be significantly reduced by switching from HFO to DF.[16,17] With the increasingly stringent global regulations on ship fuel quality, SOA production by ships may become more prominent in the future. Furthermore, it should be noted that SOA production is likely underestimated herein, as the calculation method does not account for multigenerational oxidation on semivolatile POA and SOA.[52]

Figure 5b presents the contributions of different precursor classes to predicted SOA production after 48 h of photo-oxidation under various test ship operating conditions. IVOCs contribute the vast majority of the test ship SOA production, accounting for 98.9 ± 0.9% on average. Unspeciated cyclic compounds dominate the predicted SOA production under all operating conditions. Although fuel type is the leading determinant of SOA production, the test ship operating conditions also influence SOA production. SOA production is predicted to be 0.8 and 1.0 times higher under maneuvering (include departure and arrival) and low load (15%), respectively, than under medium and high load (36%−74%) cruising conditions. Ship maneuvering and low-load cruising

DOI: 10.1021/acs.est.8b04418
Environ. Sci. Technol. 2018, 52, 12934−12942

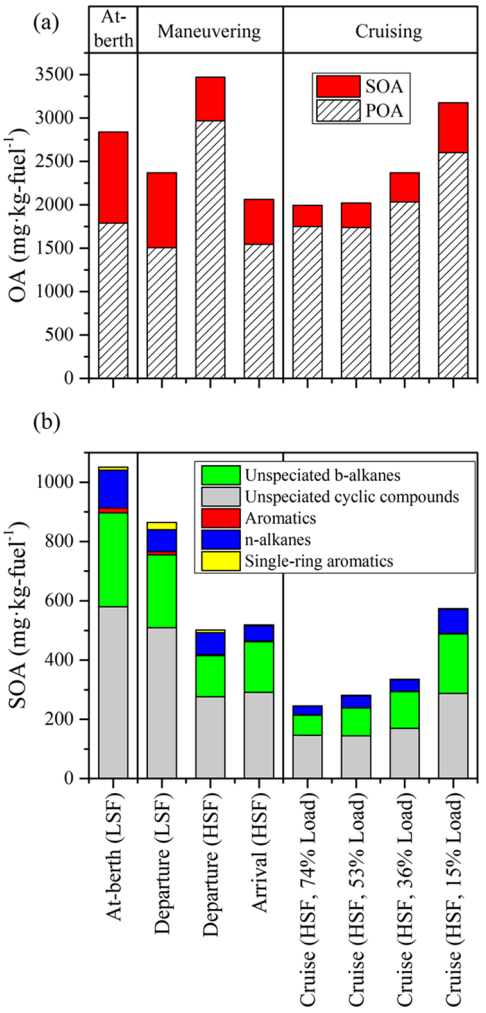

Figure 5. (a) Comparison of test ship POA emissions and predicted SOA production after 48 h of photo-oxidation under various operating conditions; (b) comparison of predicted SOA production from different classes of precursors, including VOCs and IVOCs.

operations usually occur in port or within inland rivers near urban areas, which will inevitably contribute to higher SOA production in coastal urban atmospheres.

Implications. In this study, IVOC, VOC, and POA emissions from an operating large cargo vessel were measured under real-world conditions. The results indicate that IVOCs from ships contribute considerably to total organic emissions. The average test ship IVOC EF is 1003 ± 581 mg·kg-fuel^{-1}, which is similar to the EF from diesel vehicles and much higher than that from gasoline vehicles. Combining the IVOC EFs measured in this study with the global shipping fuel consumptions (~276 Tg) predicted in a previous study for the year 2015,[39] global IVOC emissions from ships total approximately 277 ± 160 Gg. The International Energy Agency (IEA) reported global transportation sector gasoline and diesel consumptions of 935 Tg and 981 Tg, respectively, in 2017.[53] According to the gasoline and diesel vehicle IVOC EFs published by Zhao et al.,[31,32] global IVOC emissions from gasoline and diesel vehicles can be estimated at 127 Gg and 1021 Gg. This indicates that IVOC emissions from ships constitute as much as one-quarter of the total IVOC emissions from the land transportation sector and have exceeded the total emissions from gasoline vehicles. In addition, because ship emissions are concentrated primarily in coastal areas,[2] SOA formation potential from IVOC emissions will be more prominent in neighboring port cities. It is important to note that the ship has higher IVOC EFs when fueled with LSF than when fueled with HSF, which suggests that the regulations requiring the use of LSF may lead indirectly to increases in SOA formation from ships despite direct reductions in POA emissions. HFO used by ocean-going ships has been switched with DF in SECAs including the Baltic Sea, the North Sea, the English Channel, and coastal waters around the U.S., Canada, and the U.S. Caribbean Sea since 2015. By 2020, DF will be further promoted on a global scale according to IMO's regulation.[42] It can be expected that POA emissions from ocean-going ships will be effectively reduced. However, their IVOC emissions and contributions to SOA in the global atmosphere will increase. This study prospectively explores the IVOC emission characteristics from a HFO fueled ship. However, the actual contribution of ship emissions to SOA formation is closely related to the ambient conditions, including radiation, temperature, and the concentrations of precursors and OA. It is suggested that more field measurements or laboratory studies should be carried out in the future to identify the SOA contribution from ships.

■ ASSOCIATED CONTENT

Supporting Information

The Supporting Information is available free of charge on the ACS Publications website at DOI: 10.1021/acs.est.8b04418.

Descriptions of test procedures, speciated IVOC analysis, unspeciated IVOCs quantification, GC/MS analysis of organics on filters (Figures S1−S6 and Tables S1−S6) (PDF)

■ AUTHOR INFORMATION

Corresponding Authors

*Phone: +86 64085119; Fax: +86 64085119; E-mail: huangc@saes.sh.cn.

*Phone: +86 64085119; Fax: +86 64085119; E-mail: lili@saes.sh.cn.

ORCID

Cheng Huang: 0000-0001-9518-3628

Yunliang Zhao: 0000-0002-9079-5972

Li Li: 0000-0001-5575-0894

Present Address

#California Air Resources Board, Sacramento, California 95814, United States.

Notes

The authors declare no competing financial interest.

■ ACKNOWLEDGMENTS

We gratefully acknowledge the support of Shanghai Maritime University during the measurement campaign. We acknowledge the exceptional support received from all employees and crew of the ship Yuming. This work was supported by the National Key R&D Program of China (Grant 2016YFC0201501), the National Natural Science Foundation of China (Grant 21777101), the Science and Technology Commission of the Shanghai Municipality Fund Project (Grant 18DZ1203100), the Natural Science Foundation of Shanghai (18ZR1432100), and Shanghai Pujiang Program (18PJ1431400).

DOI: 10.1021/acs.est.8b04418
Environ. Sci. Technol. 2018, 52, 12934−12942

REFERENCES

(1) Corbett, J. J.; Winebrake, J. J.; Green, E. H.; Kasibhatla, P.; Eyring, V.; Lauer, A. Mortality from ship emissions: A global assessment. *Environ. Sci. Technol.* **2007**, *41* (24), 8512−8518.

(2) Eyring, V.; Isaksen, I. S. A.; Berntsen, T.; Collins, W. J.; Corbett, J. J.; Endresen, O.; Grainger, R. G.; Moldanova, J.; Schlager, H.; Stevenson, D. S. Transport impacts on atmosphere and climate: Shipping. *Atmos. Environ.* **2010**, *44*, 4735−4771.

(3) Liu, H.; Fu, M. L.; Jin, X. X.; Shang, Y.; Shindell, D.; Faluvegi, G.; Shindell, C.; He, K. B. Health and climate impacts of ocean-going vessels in East Asia. *Nat. Clim. Change* **2016**, *6* (11), 1037−1041.

(4) Zhang, Y.; Yang, X.; Brown, R.; Yang, L.; Morawska, L.; Ristovski, Z.; Fu, Q.; Huang, C. Shipping emissions and their impacts on air quality in China. *Sci. Total Environ.* **2017**, *581*−*582*, 186−198.

(5) Sofiev, M.; Winebrake, J. J.; Johansson, L.; Carr, E. W.; Prank, M.; Soares, J.; Vira, J.; Kouznetsov, R.; Jalkanen, J.; Corbett, J. J. Cleaner fuels for ships provide public health benefits with climate tradeoffs. *Nat. Commun.* **2018**, *9*, 406.

(6) Oeder, S.; Kanashova, T.; Sippula, O.; Sapcariu, S. C.; Streibel, T.; Arteaga-Salas, J. M.; Passig, J.; Dilger, M.; Paur, H.; Schlager, C.; et al. Particulate matter from both heavy fuel oil and diesel fuel shipping emissions show strong biological effects on human lung cells at realistic and comparable *in vitro* exposure conditions. *PLoS One* **2015**, *10* (6), e0126536.

(7) Becagli, S.; Sferlazzo, D. M.; Pace, G.; di Sarra, A.; Bommarito, C.; Calzolai, G.; Ghedini, C.; Lucarelli, F.; Meloni, D.; Monteleone, F.; Severi, M.; Traversi, R.; Udisti, R. Evidence for heavy fuel oil combustion aerosols from chemical analyses at the island of Lampedusa: a possible large role of ships emissions in the Mediterranean. *Atmos. Chem. Phys.* **2012**, *12* (7), 3479−3492.

(8) Gaston, C. J.; Quinn, P. K.; Bates, T. S.; Gilman, J. B.; Bon, D. M.; Kuster, W. C.; Prather, K. A. The impact of shipping, agricultural, and urban emissions on single particle chemistry observed aboard the R/V Atlantis during CalNex. *J. Geophys. Res. Atmos.* **2013**, *118* (10), 5003−5017.

(9) Yau, P. S.; Lee, S. C.; Cheng, Y.; Huang, Y.; Lai, S. C.; Xu, X. H. Contribution of ship emissions to the fine particulate in the community near an international port in Hong Kong. *Atmos. Res.* **2013**, *124*, 61−72.

(10) Liu, Z. M.; Lu, X. H.; Feng, J. L.; Fan, Q. Z.; Zhang, Y.; Yang, X. Influence of ship emissions on urban air quality: A comprehensive study using highly time-resolved online measurements and numerical simulation in Shanghai. *Environ. Sci. Technol.* **2017**, *51* (1), 202−211.

(11) Agrawal, H.; Malloy, Q. G. J.; Welch, W. A.; Miller, J. W.; Cocker, D. R., III In-use gaseous and particulate matter emissions from a modern ocean going container vessel. *Atmos. Environ.* **2008**, *42*, 5504−5510.

(12) Lack, D. A.; Corbett, J. J.; Onasch, T.; Lerner, B.; Massoli, P.; Quinn, P. K.; Bates, T. S.; Covert, D. S.; Coffman, D.; Sierau, B.; et al. Particulate emissions from commercial shipping: Chemical, physical, and optical properties. *J. Geophys. Res.* **2009**, *114*, D00F04.

(13) Lack, D. A.; Corbett, J. J. Black carbon from ships: a review of the effects of ship speed, fuel quality and exhaust gas scrubbing. *Atmos. Chem. Phys.* **2012**, *12* (9), 3985−4000.

(14) Moldanová, J.; Fridell, E.; Winnes, H.; Holmin-Fridell, S.; Boman, J.; Jedynska, A.; Tishkova, V.; Demirdjian, B.; Joulie, S.; Bladt, H.; Ivleva, N. P.; Niessner, R. Physical and chemical characterisation of PM emissions from two ships operating in European emission control areas. *Atmos. Meas. Tech.* **2013**, *6* (12), 3577−3596.

(15) Huang, C.; Hu, Q. Y.; Wang, H. Y.; Qiao, L. P.; Jing, S. A.; Wang, H. L.; Zhou, M.; Zhu, S. H.; Ma, Y. G.; Lou, S. R.; Li, L.; Tao, S. K.; Li, Y. J.; Lou, D. M. Emission factors of particulate and gaseous compounds from a large cargo vessel operated under real-world conditions. *Environ. Pollut.* **2018**, *242*, 667−674.

(16) Lack, D. A.; Cappa, C. D.; Langridge, J.; Bahreini, R.; Buffaloe, G.; Brock, C.; Cerully, K.; Coffman, D.; Hayden, K.; Holloway, J.; Lerner, B.; Massoli, P.; Li, S. M.; McLaren, R.; Middlebrook, A. M.; Moore, R.; Nenes, A.; Nuaaman, I.; Onasch, T. B.; Peischl, J.; Perring, A.; Quinn, P. K.; Ryerson, T.; Schwartz, J. P.; Spackman, R.; Wofsy, S. C.; Worsnop, D.; Xiang, B.; Williams, E. Impact of fuel quality regulation and speed reductions on shipping emissions: Implications for climate and air quality. *Environ. Sci. Technol.* **2011**, *45* (20), 9052−9060.

(17) Sippula, O.; Stengel, B.; Sklorz, M.; Streibel, T.; Rabe, R.; Orasche, J.; Lintelmann, J.; Michalke, B.; Abbaszade, G.; Radischat, C.; Gröger, T.; Schnelle-Kreis, J.; Harndorf, H.; Zimmermann, R. Particle emissions from a marine engine: chemical composition and aromatic emission profiles under various operating conditions. *Environ. Sci. Technol.* **2014**, *48* (19), 11721−11729.

(18) Radischat, C.; Sippula, O.; Stengel, B.; Klingbeil, S.; Sklorz, M.; Rabe, R.; Streibel, T.; Harndorf, H.; Zimmermann, R. Real-time analysis of organic compounds in ship engine aerosol emissions using resonance-enhanced multiphoton ionization and proton transfer mass spectrometry. *Anal. Bioanal. Chem.* **2015**, *407* (20), 5939−5951.

(19) Czech, H.; Stengel, B.; Adam, T.; Sklorz, M.; Streibel, T.; Zimmermann, R. A chemometric investigation of aromatic emission profiles from a marine engine in comparison with residential wood combustion and road traffic: Implications for source apportionment inside and outside sulphur emission control areas. *Atmos. Environ.* **2017**, *167*, 212−222.

(20) Donahue, N. M.; Robinson, A. L.; Stanier, C. O.; Pandis, S. N. Coupled partitioning, dilution, and chemical aging of semivolatile organics. *Environ. Sci. Technol.* **2006**, *40* (8), 2635−2643.

(21) Robinson, A. L.; Donahue, N. M.; Shrivastava, M. K.; Weitkamp, E. A.; Sage, A. M.; Grieshop, A. P.; Lane, T. E.; Pierce, J. R.; Pandis, S. N. Rethinking organic aerosols: Semivolatile emissions and photochemical aging. *Science* **2007**, *315* (5816), 1259−1262.

(22) Chan, A. W. H.; Kautzman, K. E.; Chhabra, P. S.; Surratt, J. D.; Chan, M. N.; Crounse, J. D.; Kurten, A.; Wennberg, P. O.; Flagan, R. C.; Seinfeld, J. H. Secondary organic aerosol formation from photooxidation of naphthalene and alkylnaphthalenes: Implications for oxidation of intermediate volatility organic compounds (IVOCs). *Atmos. Chem. Phys.* **2009**, *9* (9), 3049−3060.

(23) Lim, Y. B.; Ziemann, P. J. Effects of molecular structure on aerosol yields from OH radical-initiated reactions of linear, branched, and cyclic alkanes in the presence of NO_x. *Environ. Sci. Technol.* **2009**, *43* (7), 2328−2334.

(24) Presto, A. A.; Miracolo, M. A.; Donahue, N. M.; Robinson, A. L. Secondary organic aerosol formation from high-NO_x photo-oxidation of low volatility precursors: n-alkanes. *Environ. Sci. Technol.* **2010**, *44* (6), 2029−2034.

(25) Tkacik, D. S.; Presto, A. A.; Donahue, N. M.; Robinson, A. L. Secondary Organic Aerosol Formation from Intermediate-Volatility Organic Compounds: Cyclic, Linear, and Branched Alkanes. *Environ. Sci. Technol.* **2012**, *46* (16), 8773−8781.

(26) Hunter, J. F.; Carrasquillo, A. J.; Daumit, K. E.; Kroll, J. H. Secondary organic aerosol formation from acyclic, monocyclic, and polycyclic alkanes. *Environ. Sci. Technol.* **2014**, *48* (17), 10227−10234.

(27) Gentner, D. R.; Isaacman, G.; Worton, D. R.; Chan, A. W. H.; Dallmann, T. R.; Davis, L.; Liu, S.; Day, D. A.; Russell, L. M.; Wilson, K. R.; Weber, R.; Guha, A.; Harley, R. A.; Goldstein, A. H. Elucidating secondary organic aerosol from diesel and gasoline vehicles through detailed characterization of organic carbon emissions. *Proc. Natl. Acad. Sci. U. S. A.* **2012**, *109* (45), 18318−18323.

(28) Tkacik, D. S.; Lambe, A. T.; Jathar, S.; Li, X.; Presto, A. A.; Zhao, Y. L.; Blake, D.; Meinardi, S.; Jayne, J. T.; Croteau, P. L.; Robinson, A. L. Secondary organic aerosol formation from in-use motor vehicle emissions using a potential aerosol mass reactor. *Environ. Sci. Technol.* **2014**, *48* (19), 11235−11242.

(29) Stroud, C. A.; Liggio, J.; Zhang, J.; Gordon, M.; Staebler, R. M.; Makar, P. A.; Zhang, J. H.; Li, S. M.; Mihele, C.; Lu, G.; Wang, D. K.; Wentzell, J.; Brook, J. R.; Evans, G. J. Rapid organic aerosol formation downwind of a highway: Measured and model results from the FEVER study. *J. Geophys. Res.* **2014**, *119* (3), 1663−1679.

(30) Gentner, D. R.; Jathar, S. H.; Gordon, T. D.; Bahreini, R.; Day, D. A.; El Haddad, I.; Hayes, P. L.; Pieber, S. M.; Platt, S. M.; de

DOI: 10.1021/acs.est.8b04418
Environ. Sci. Technol. 2018, 52, 12934−12942

Gouw, J.; et al. Review of urban secondary organic aerosol formation from gasoline and diesel motor vehicle emissions. *Environ. Sci. Technol.* **2017**, *51* (3), 1074−1093.
(31) Zhao, Y.; Nguyen, N. T.; Presto, A. A.; Hennigan, C. J.; May, A. A.; Robinson, A. L. Intermediate volatility organic compound emissions from on-road diesel vehicles: chemical composition, emission factors, and estimated secondary organic aerosol production. *Environ. Sci. Technol.* **2015**, *49* (19), 11516−11526.
(32) Zhao, Y.; Nguyen, N. T.; Presto, A. A.; Hennigan, C. J.; May, A. A.; Robinson, A. L. Intermediate volatility organic compound emissions from on-road gasoline vehicles and small off-road gasoline engines. *Environ. Sci. Technol.* **2016**, *50* (8), 4554−4563.
(33) Zhao, Y.; Kreisberg, N. M.; Worton, D. R.; Teng, A. P.; Hering, S. V.; Goldstein, A. H. Development of an in situ thermal desorption gas chromatography instrument for quantifying atmospheric semi-volatile organic compounds. *Aerosol Sci. Technol.* **2013**, *47* (3), 258−266.
(34) Zhao, Y. L.; Hennigan, C. J.; May, A. A.; Tkacik, D. S.; de Gouw, J. A.; Gilman, J. B.; Kuster, W. C.; Borbon, A.; Robinson, A. L. Intermediate-Volatility Organic Compounds: A Large Source of Secondary Organic Aerosol. *Environ. Sci. Technol.* **2014**, *48* (23), 13743−13750.
(35) Jathar, S. H.; Gordon, T. D.; Hennigan, C. J.; Pye, H. O. T.; Pouliot, G.; Adams, P. J.; Donahue, N. M.; Robinson, A. L. Unspeciated organic emissions from combustion sources and their influence on the secondary organic aerosol budget in the United States. *Proc. Natl. Acad. Sci. U. S. A.* **2014**, *111* (29), 10473−10478.
(36) Hodzic, A.; Jimenez, J. L.; Madronich, S.; Canagaratna, M. R.; DeCarlo, P. F.; Kleinman, L.; Fast, J. Modeling organic aerosols in a megacity: potential contribution of semi-volatile and intermediate volatility primary organic compounds to secondary organic aerosol formation. *Atmos. Chem. Phys.* **2010**, *10* (12), 5491−5514.
(37) Pye, H. O. T.; Seinfeld, J. H. A global perspective on aerosol from low-volatility organic compounds. *Atmos. Chem. Phys.* **2010**, *10* (9), 4377−4401.
(38) Zhao, B.; Wang, S. X.; Donahue, N. M.; Jathar, S. H.; Huang, X. F.; Wu, W. J.; Hao, J. M.; Robinson, A. L. Quantifying the effect of organic aerosol aging and intermediate volatility emissions on regional scale aerosol pollution in China. *Sci. Rep.* **2016**, *6*, 28815.
(39) Johansson, L.; Jalkanen, J.; Kukkonen, J. Global assessment of shipping emissions in 2015 on a high spatial and temporal resolution. *Atmos. Environ.* **2017**, *167*, 403−415.
(40) Hoesly, R. M.; Smith, S. J.; Feng, L.; Klimont, Z.; Janssens-Maenhout, G.; Pitkanen, T.; Seibert, J. J.; Vu, L.; Andres, R. J.; Bolt, R. M.; et al. Historical (1750−2014) anthropogenic emissions of reactive gases and aerosols from the Community Emissions Data System (CEDS). *Geosci. Model Dev.* **2018**, *11* (1), 369−408.
(41) Li, C.; Borken-Kleefeld, J.; Zheng, J.; Yuan, Z.; Ou, J.; Li, Y.; Wang, Y.; Xu, Y. Decadal evolution of ship emissions in China from 2004 to 2013 by using an integrated AIS-based approach and projection to 2040. *Atmos. Chem. Phys.* **2018**, *18* (8), 6075−6093.
(42) International Maritime Organization (IMO). *Sulphur oxides (SO_x). Regulation 14*; 2017.
(43) Lack, D. A.; Cappa, C. D.; Langridge, J.; Bahreini, R.; Buffaloe, G.; Brock, C.; Cerully, K.; Coffman, D.; Hayden, K.; Holloway, J.; Lerner, B.; Massoli, P.; Li, S. M.; McLaren, R.; Middlebrook, A. M.; Moore, R.; Nenes, A.; Nuaaman, I.; Onasch, T. B.; Peischl, J.; Perring, A.; Quinn, P. K.; Ryerson, T.; Schwartz, J. P.; Spackman, R.; Wofsy, S. C.; Worsnop, D.; Xiang, B.; Williams, E. Impact of fuel quality regulation and speed reductions on shipping emissions: Implications for climate and air quality. *Environ. Sci. Technol.* **2011**, *45* (20), 9052−9060.
(44) Celo, V.; Dabek-Zlotorzynska, E.; McCurdy, M. Chemical characterization of exhaust emissions from selected Canadian marine vessels: The case of trace metals and lanthanoids. *Environ. Sci. Technol.* **2015**, *49* (8), 5220−5226.
(45) Streibel, T.; Schnelle-Kreis, J.; Czech, H.; Harndorf, H.; Jakobi, G.; Jokiniemi, J.; Karg, E.; Lintelmann, J.; Matuschek, G.; Michalke, B.; Müller, L.; Orasche, J.; Passig, J.; Radischat, C.; Rabe, R.; Reda, A.; Rüger, C.; Schwemer, T.; Sippula, O.; Stengel, B.; Sklorz, M.; Torvela, T.; Weggler, B.; Zimmermann, R. Aerosol emissions of a ship diesel engine operated with diesel fuel or heavy fuel oil. *Environ. Sci. Pollut. Res.* **2017**, *24* (12), 10976−10991.
(46) Lyu, X. P.; Guo, H.; Cheng, H. R.; Wang, X. M.; Ding, X.; Lu, H. X.; Yao, D. W.; Xu, C. Observation of SOA tracers at a mountainous site in Hong Kong: Chemical characteristics, origins and implication on particle growth. *Sci. Total Environ.* **2017**, *605*, 180−189.
(47) Li, Y. J.; Wang, J. H.; Ren, B. N.; Wang, H. L.; Qiao, L. P.; Zhu, J. P.; Li, L. The characteristics of atmospheric phthalates in Shanghai: A haze case study and human exposure assessment. *Atmos. Environ.* **2018**, *178*, 80−86.
(48) Chow, J. C.; Watson, J. G.; Chen, L. W. A.; Chang, M. C. O.; Robinson, N. F.; Trimble, D.; Kohl, S. The IMPROVE_A temperature protocol for thermal/optical carbon analysis: maintaining consistency with a long-term database. *J. Air Waste Manage. Assoc.* **2007**, *57* (9), 1014−1023.
(49) Turpin, B. J.; Lim, H. J. Species contributions to $PM_{2.5}$ mass concentrations: Revisiting common assumptions for estimating organic mass. *Aerosol Sci. Technol.* **2001**, *35* (1), 602−610.
(50) May, A. A.; Nguyen, N. T.; Presto, A. A.; Gordon, T. D.; Lipsky, E. M.; Karve, M.; Gutierrez, A.; Robertson, W. H.; Zhang, M.; Brandow, C.; Chang, O.; Chen, S.; Cicero-Fernandez, P.; Dinkins, L.; Fuentes, M.; Huang, S.; Ling, R.; Long, J.; Maddox, C.; Massetti, J.; McCauley, E.; Miguel, A.; Na, K.; Ong, R.; Pang, Y.; Rieger, P.; Sax, T.; Truong, T.; Vo, T.; Chattopadhyay, S.; Maldonado, H.; Maricq, M. M.; Robinson, A. L. Gas- and particle-phase primary emissions from in-use, on-road gasoline and diesel vehicles. *Atmos. Environ.* **2014**, *88*, 247−260.
(51) Zhao, Y. L.; Saleh, R.; Saliba, G.; Presto, A. A.; Gordon, T. D.; Drozd, G. T.; Goldstein, A. H.; Donahue, N. M.; Robinson, A. L. Reducing secondary organic aerosol formation from gasoline vehicle exhaust. *Proc. Natl. Acad. Sci. U. S. A.* **2017**, *114* (27), 6984−4989.
(52) Kroll, J. H.; Seinfeld, J. H. Chemistry of secondary organic aerosol: Formation and evolution of low-volatility organics in the atmosphere. *Atmos. Environ.* **2008**, *42* (16), 3593−3624.
(53) International Energy Agency (IEA). *Oil Information 2017*; Paris, 2018.

DOI: 10.1021/acs.est.8b04418
Environ. Sci. Technol. 2018, 52, 12934−12942